University of Reading

Self-assembly and intracellular delivery of DNA by a truncated fragment derived from the Trojan peptide Penetratin

Article

Accepted Version

Mello, L. R., Hamley, I. W., Castelletto, V., Garcia, B. B. M., Lourenço, T. C., Vassiliades, S. V., Alves, W. A., Han, S. W. and Silva, E. R. (2020) Self-assembly and intracellular delivery of DNA by a truncated fragment derived from the Trojan peptide Penetratin. Soft Matter, 16 (20). pp. 4746-4755. ISSN 1744-683X doi: https://doi.org/10.1039/D0SM00347F Available at https://centaur.reading.ac.uk/91719/

It is advisable to refer to the publisher's version if you intend to cite from the work. See Guidance on citing.
Published version at: http://dx.doi.org/10.1039/D0SM00347F
To link to this article DOI: http://dx.doi.org/10.1039/D0SM00347F

Publisher: Royal Society of Chemistry

All outputs in CentAUR are protected by Intellectual Property Rights law, including copyright law. Copyright and IPR is retained by the creators or other copyright holders. Terms and conditions for use of this material are defined in the End User Agreement.

www.reading.ac.uk/centaur

University of Reading

CentAUR

Central Archive at the University of Reading

Reading's research outputs online

Self-assembly and Intracellular Delivery of DNA by a Truncated Fragment Derived from the *Trojan* Peptide Penetratin

Lucas R. Mello,[a] Ian W. Hamley,[b] Valeria Castelletto,[b] Bianca B. M. Garcia,[a] Thiago C. Lourenço,[a] Sandra V. Vassiliades,[c] Wendel A. Alves,[c] Sang W. Han,[a] and Emerson R. Silva[a*]

[a] Departamento de Biofísica, Universidade Federal de São Paulo, São Paulo 04023-062, Brazil;
[b] Department of Chemistry, University of Reading, Reading RGD 6AD, United Kingdom;
[c] Centro de Ciências Naturais e Humanas, Universidade Federal do ABC, Santo André 09210-580, Brazil.

ABSTRACT

Penetratin is a short *Trojan* peptide that attracts great interest in biomedical research for its capacity to translocate biological membranes. Herein, we study in detail both self-assembly and intracellular delivery of DNA by the heptamer KIWFQNR, a truncated peptide derived from *Penetratin*. This shortened sequence possesses a unique design with bolaamphiphilic characteristics that preserves the longest noncationic amino acid portion found in *Penetratin.* These features convey amphipathicity to assist self-assembly and make it a suitable model for exploring the role of hydrophobic residues for peptide interaction and cell uptake. We show that the fragment forms peptiplexes (i.e., peptide-DNA complexes), and aggregates into long nanofibers with clear β-sheet signature. The supramolecular structure of nanofibers likely comprises DNA cores surrounded by a peptide shell for which the double helix behaves as a template and induces fibrillization. A nucleation and growth mechanism proceeding through liquid-liquid phase separation of coacervates is proposed for describing the self-assembly of peptiplexes. We also demonstrate that peptiplexes deliver double-stranded 200bp DNA into HeLa cells, indicating its potential for preparing non-viral vectors for oligonucleotides through noncovalent strategies. Since the main structural features of native *Penetratin* are conserved in this simpler fragment, our findings also highlight the role of uncharged amino acids for structuration, and thus for the ability of *Penetratin* to cross cell membranes.

***Corresponding author:** er.silva@unifesp.br

INTRODUCTION

Cell-penetrating peptides (CPPs), often also called *Trojan* peptides, are considered one of the most promising candidates for intracellular delivery of bioactive molecules and constitute a major peptide class in future development of therapeutics.[1–3] CPPs have been serendipitously discovered about three decades ago during researches on the function of transcriptional regulators in gene activity.[4,5] One striking *Trojan* peptide that emerged from these earlier investigations is *Penetratin*, a 16-mer sequence present in the *Antennapedia* homeodomain of *Drosophila melanogaster*.[1,6] This sequence exhibits strong tropism towards biological membranes[7] and since its discovery it has been extensively investigated as a transporter for a variety of molecular cargoes.[8–10] Recently, *Penetratin* has been employed in new strategies to overcome the blood brain barrier,[11,12] to promote intraocular delivery[9,13,14] and for the production of novel cancer therapeutics.[10,15] Particularly, the DNA-binding characteristics of the parent *Antennapedia* homeoprotein has inspired the development of *Penetratin*-based vectors for delivery of nucleic acid payloads which has potential for use in gene therapy.[9,16,17]

The *Penetratin* peptide is composed of the following amino acid sequence: RQIKIWFQNRRMKWKK.[6] Similar to vast majority of *Trojan* sequences,[3,18] it is composed of several basic residues making it very competent for noncovalent interactions with anionic species such as DNA. In contrast, it also displays a few hydrophobic amino acids that lead to a "dual mode" of interaction with lipid membranes.[19,20] The ability of *Penetratin* to form ordered aggregates in the presence of anionic surfactants has motivated the study of the synergism between this peptide and lipids.[19,21,22] Although understanding on the exact mechanisms by which *Penetratin* translocates cell membranes is a still evolving process, it has been shown that interaction with negatively-charged phospholipids is mainly driven by electrostatic attraction, followed by limited insertion of peptide into bilayers.[23,24] In addition, it has been demonstrated

that amphipathicity of *Penetratin* is not sufficient to allow deep insertion into biomembranes,[25] and in this case permeation has been proposed to occur through a process involving the formation of inverted micelles.[26]

In the present work, we study the heptamer KIWFQNR, a shortened fragment derived from *Penetratin.* The chemical structure of the peptide is presented in Figure 1, and it shows several peculiarities that have motivated our choice: first, it contains the longest hydrophobic segment in the *Penetratin* strand. Since structuration capabilities of *Penetratin* have been identified as an intermediate step for its translocation capacity,[24,26,27] this hydrophobic portion should play a relevant functional role in the permeation properties of the *Trojan* peptide. Secondly, it carries a tryptophan residue which is well-known to be necessary for efficient membrane translocation by *Penetratin*.[28–30] As shown below, tryptophan also provides a powerful probe to track physicochemical properties of the peptide. Finally, it possesses cationic residues at both termini, enabling electrostatic binding to anionic species (e.g., DNA or biomembranes), and conveying a bolaamphiphile-like design that could assist self-assembly into ordered structures. Putting these features together, it is of great interest to investigate the role of this hydrophobic segment in relation to the structuration and cell penetration behavior of the parent *Penetratin* peptide.

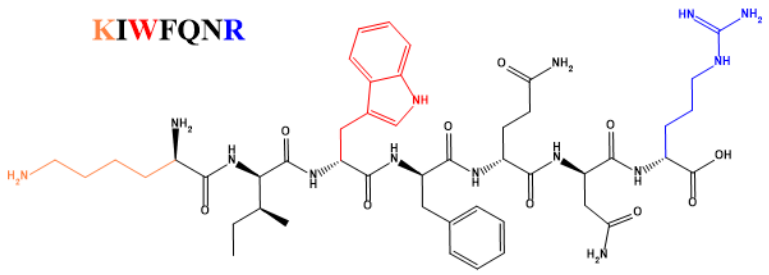

Figure 1: Chemical structure of the peptide investigated in this work (*KIW7*). Cationic residues at both termini and the tryptophan indole group in the middle of the sequence appear colored.

MATERIALS AND METHODS

Peptide synthesis, reagents and sample preparation: The heptameric sequence NH_2-KIWFQNR-COOH (K: lysine, I: isoleucine, W: tryptophan, F: phenylalanine, Q: glutamine, N: asparagine, R: arginine) was synthetized using routine solid-phase approaches as described elsewhere.[31,32] For simplicity, henceforth, the heptameric sequence will be referred to by the shortened form *KIW7*. The peptide product has been obtained as a TFA salt, being characterized by liquid chromatography coupled to mass spectroscopy assays which revealed purity and molecular mass, respectively, of 97.7% and 991.6 g/mol (calculated M_w = 991.15 Da). The corresponding chromatogram and mass spectrum are shown in the ESI file (Figure S1). Calf thymus DNA, containing 10-20 kb, was acquired from Sigma-Aldrich (product code D1501). These polymerized chains were broken into fragments with ~200 bp through ultrasonication on a Diagenode Bioruptor as previously described,[33–35] which were characterized by agarose electrophoresis (ESI file, Fig. S2A). These 200 bp DNA fragments possess calculated length at $L = 200 \times 0.33 \sim 67$ nm, close to the to the persistence length of double-stranded DNA.[36] SAXS measurements on 200 bp DNA solutions indicated the presence of rod-like structures, with diameters around 2.6 nm, consistent with the thickness of DNA duplexes plus a hydration shell (see ESI, Fig. S2B).[36] Plasmid vector, pEGFP-N3, was acquired from Clontech (Mountain View, CA, USA) and DH5a bacteria was used for transformation and amplification.[37] For large scale production of this plasmid, Endo-free Gigaprep kit from Qiagen (Hilden, Germany) was used following the manufacturer's instructions. The purified plasmid was resuspended in water and maintained in -20 ºC freezer until its use. Stock solutions were prepared by weighing lyophilized peptides and 200 bp DNA into test tubes and re-suspending in ultrapure water (or D_2O). Peptides formed transparent samples immediately upon dissolution whereas concentrated solutions prepared from lyophilized 200 bp DNA required a few hours of alternating vigorous vortexing cycles to assist homogenization. All preparations were kept in

the fridge (4 °C). Complexes were prepared by mixing defined amounts from stock solutions to obtain desired molar ratios between cationic charges on peptide side chains and anionic charges at phosphate groups of DNA (N^+:P^- ratio). Since our preparations were close to neutral pH, a net charge +2 per peptide strand and -2 per DNA base pair was assumed. **Spectrofluorimetry Assays**: fluorescence assays were carried out using a Shimadzu F2500 instrument. Samples with concentrations ranging from 2.2 mg/ml down to 3×10^{-4} mg/ml were prepared through serial dilutions in water. The presence of a tryptophan residue in the amino acid sequence allowed to use its intrinsic fluorescence to assess changes in the aggregation state of the peptide. Samples were irradiated with λ_{exc} = 280 nm and emission spectra were acquired in the range 300–500 nm. Excitation and emission slits were set for the best achievable signal/noise ratio. **Circular Dichroism (CD).** Aqueous solutions containing peptides at 0.1 mg/ml were placed into Hellma cells with 1 mm path length. The peptide solutions were titrated with 200bp DNA aliquots from a concentrated solution in order to scan a range of N^+:P^- ratios below and above the point of molar equivalence between positive and negative charges. CD data were collected in the range 190 – 260 nm, in steps of 1 nm and 1 s per step, using four accumulations. All data have been background-subtracted prior to further treatment, and conversion into ellipticity units has been performed considering the mean residual weight, peptide concentration and pathlength of cuvette used in the experiments. Only data exhibiting absorbance < 2 were considered for analysis. Fourier filtering (7 points window) was used to minimize noise. **Small-angle X-ray Scattering and fiber X-ray diffraction.** SAXS data were collected on SAXS-1 beamline at LNLS (Campinas, Brazil), using X-rays energy of 8 KeV and q-range 0.12 nm^{-1} < q < 3.0 nm^{-1}. Samples were left to equilibrate for 2-3 days at 4 °C prior to SAXS experiments and peptide concentrations of about 5 mg/ml were used in the preparations, while the amount of 200bp DNA was adjusted to match the 1:1 peptide-to-phosphate charge ratio. Aliquots 300 μl of solutions were carefully injected between mica windows of a cell

holder with 1 mm pathlength. Ten frames, 30 s each, were acquired and, since no radiation damage was detected, they were averaged, and background subtracted. All experiments were carried out at room temperature. Samples for fiber X-ray diffraction were prepared by suspending droplets from concentrated *KIW7*/pDNA solutions (5 mg/ml) between wax-coated capillaries. The capillaries with the suspended droplets were carefully placed inside Petri dishes, sealed with parafilm, and left to dry for about 1 week in the fridge. The resulting stalks were positioned onto a RAXIS IV++ diffractometer and irradiated with 8 keV X-rays. The sample-to-detector distance was kept at 50 mm and data were collected by a Saturn 992 CCD camera. 1D spectra were obtained by using Fit2D software. **Atomic Force Microscopy**: a Park NX10 atomic force microscope was used for data collection at LNNano (CNPEM, Campinas – Brazil). Samples were prepared by casting about 20 μl from peptides or 1:1 peptide:DNA solutions onto the surface of freshly cleaved mica. Samples were left to rest for about 5 minutes and then rinsed to wash out excess of solution. Substrates were left to dry overnight into desiccators prior to measurements which have been performed in tapping mode, with a cantilever operating at ~240 kHz. Image visualization and enhancement was performed with software Gwyddion. **Cryogenic transmission electron microscopy (TEM).** Transmission electron microscopy imaging was carried out on a JEOL 2100 FEG-TEM microscope at LNNano, Campinas, Brazil. Grids for cryo-TEM samples have been treated with a plasma glow discharge to enhance adhesion of particles. Aliquots 3 μl from 5 mg/ml peptide solutions were cast onto lacey carbon grids (300 mesh), and quickly plunged into liquid ethane cooled by liquid nitrogen using a Vitribot device. The grids were transferred into the microscope under refrigerated conditions and kept at cryogenic temperatures until the end of analyses. The microscope operated at an acceleration voltage of 200 keV and further data treatment was performed with Image J software. **Cell Culture and Fluorescence Imaging using Confocal Microscopy**: HeLa cells were cultured in Dulbecco's modified Eagle medium (DMEM) with

the addition of 10% of fetal bovine serum and 2 mM of glutamine (ThermoFisher) and maintained in a humidified chamber with 5% CO_2 at 37 ºC. In each well of 24-well plates, a sterilized glass coverslip was placed on the bottom and $5x10^4$ cells were added and maintained for 24 hours with 5% CO_2 at 37 ºC. Culture plates were washed three times with PBS to remove excess of serum and cell debris. The complexes formed between *KIW7* and 200bp DNA in serum-free DMEM were added in the plates and incubated for 4 hours. After this, plates were washed with PBS three times to remove unadhered cells and unbonded complexes. The adhered cells were fixated with 4% paraformaldehyde and stained with DAPI fluorescent dye (Thermo Scientific) in PBS for five minutes to stain cell nuclei. After this period, they were washed again three times with PBS and analyzed by confocal microscopy (Leica TCS SP8, Mannheim, Germany).

RESULTS AND DISCUSSION

Steady-state fluorimetry: association to anionic species

Since the indole group of the tryptophan side chain is highly sensitive to local conditions of the molecule, intrinsic fluorescence of *KIW7* could be used to extract valuable information on its chemical environment and provide insights into the structure. *KIW7* possesses a bolaamphiphilic design, therefore, this peptide is likely prone to self-aggregate in aqueous solution. In Figure 2A, we show a series of fluorescence spectra from aqueous solutions at different concentrations whose emission spectra (inset) are characterized by a broad peak at λ_{max} ~ 350 nm. Fluorescence intensities are modulated by peptide concentration, increasing to such an extent that solutions at ~ 0.2 mg/ml exhibit a violet glow under UV light (insets in 2A). To get further understanding on this emission behavior, peak intensities have been plotted as a function of logarithm of peptide concentration. This plot discloses two very

distinct regimes, with emission showing moderate increase in the dilute domain and strong growth in the concentrated range. The data suggest stabilization of fluorescence at higher concentrations (i.e., > 0.2 mg/ml), possibly correlated to appearance of peptide aggregates leading to light scattering.[38] The overall shape of the curve is well described by a sigmoidal function with inversion point at 0.05 mg/ml, which is interpreted as a putative critical aggregation concentration (CAC) for *KIW7*.

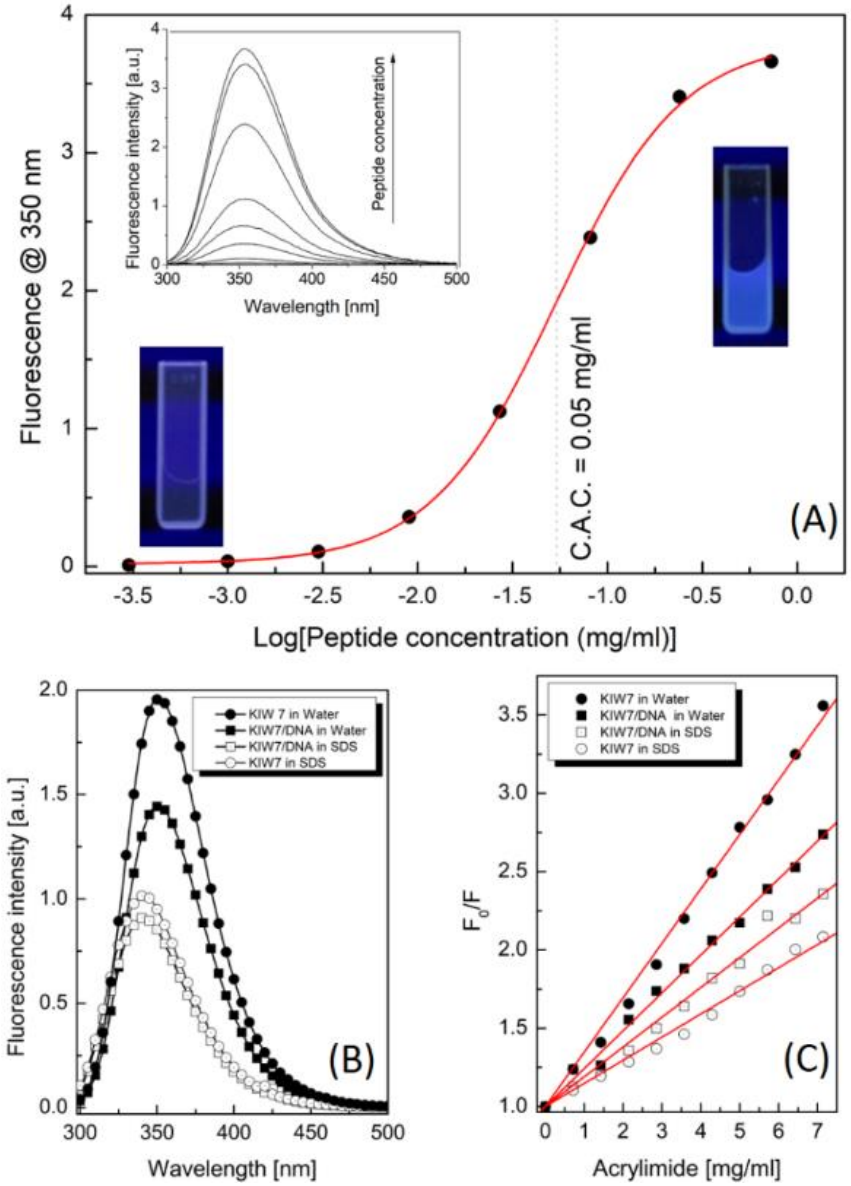

Figure 2: (A) Tryptophan fluorescence from *KIW7* solutions. Peak intensities at λ_{max} = 350 nm have been fitted as a function of peptide concentration and fitted to a Boltzmann function with

inversion point at 0.05 mg/ml. Insets: spectra used to construct the sigmoidal plot and photographs from solutions under UV light. (B) Emission spectra from 0.05 mg/ml *KIW7* solutions in the presence or absence of 200bp DNA and SDS micelles. (C) Stern-Volmer plots from acrylamide quenching assays in solutions containing *KIW7* (circles) or peptiplexes (squares), either in water (filled symbols) or in 29 mg/ml SDS micelles (open symbols).

Tryptophan fluorescence could be used to probe interactions between *KIW7* and other molecules.[39] Since this heptamer is a cationic fragment derived from *Penetratin*, a peptide with recognized cell-penetrating capabilities useful for intracell delivery, we investigated its interaction with 200bp DNA and with sodium dodecyl sulfate (SDS) micelles. DNA is a potentially bioactive load highly attractive for gene therapy, whereas SDS micelles are extensively used as a first approximation for surfactant interfaces to mimic interaction between proteins and biomembranes due to the anionic nature of their headgroups.[40–43] Figure 2B shows fluorescence spectra from mixtures containing 0.05 mg/ml *KIW7* either in the presence of 200bp DNA or co-solubilized with SDS micelles. The results show a blue shift of about 10 nm in the emission spectrum in the presence of SDS, indicating that indole moieties in these samples are surrounded by a hydrophobic environment, and suggesting that tryptophan residues are partially shielded from the aqueous phase.[44] In the absence of SDS micelles, co-solubilization with 200bp DNA does not induce peak shifts, however, a remarkable decrease of intensity is observed. We verified that absorbance at λ = 280 nm is marginally higher in samples containing DNA, therefore such a strong decline in fluorescence likely results from association between *KIW7* and DNA which presumably diminishes the rotational freedom of tryptophan side chains.[39] Interestingly, interaction with SDS micelles is also observed in samples containing *KIW7*/200bp DNA at equal molar charge ratio, which is an indication that these peptiplexes could be able to interact with anionic surfactant interfaces even in the absence of strong electrostatic attraction.

We also investigated accessibility of tryptophan residues through acrylamide quenching assays. In Figure 2C, Stern-Volmer plots are shown along with linear fits according to the equation $F_0/F = 1 + K_{SV}[Q]$, where F_0 is the fluorescence intensity of unquenched solutions, F is the emission at a given acrylamide concentration [Q] and K_{SV} is the Stern-Volmer constant that provides a quantitative index for quenching efficiency.[39] Solutions containing only *KIW7* in water presented K_{SV} = 24.8 ± 0.3 M^{-1}, whereas those containing the peptide in the presence of SDS micelles exhibited the lowest quenching constant values at K_{SV} = 10.5 ± 0.2 M^{-1}. Not surprisingly, lower quenching constants have been found for SDS-containing samples, reinforcing that peptides are partially buried in hydrophobic core of micelles and this suggests that *KIW7* is a good candidate for interacting with cell membranes. In the case of samples containing peptiplexes prepared at equal peptide-to-DNA charge ratio, K_{SV} constants present intermediate values and have been found at 17.3 ± 0.2 and 13.6 ± 0.3 M^{-1}, respectively, for preparations in water and SDS micelles. These results indicate that although complexation with 200bp DNA decreases the strength of interaction with micelles, association is still possible likely due to the amphipathic nature of the peptide. These findings represent initial physicochemical evidence supporting *KIW7* as a potential candidate to prepare peptiplexes for intracell delivery of DNA.

Circular dichroism assays: secondary structure transitions

Circular dichroism (CD) assays were performed to investigate the secondary structure of *KIW7* peptide. The CD spectrum from *KIW7* in water (Figure 3A) comprises shallow positive peak at ~195 nm followed by a sharp negative rotation at ~205 nm, corresponding to a red shifted signature of disordered conformations.[45,46] A positive maximum near 225 nm is likely correlated to electronic transitions of aromatic side chains of tryptophan and

phenylalanine residues.[45,47] The presence of disordered conformations in *KIW7* is consistent with secondary structure displayed by *Penetratin*, which also exhibits such structures in aqueous solutions.[23,24]

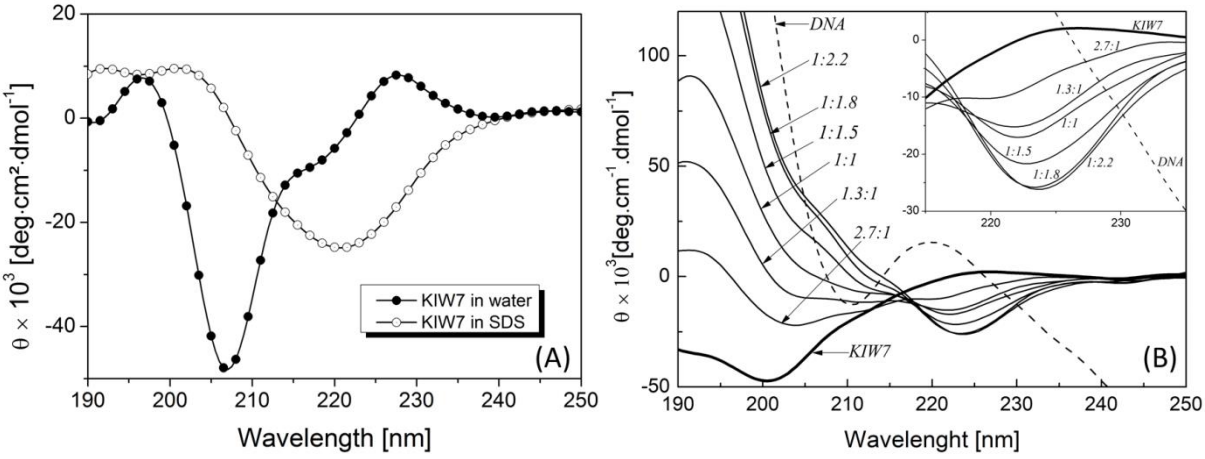

Figure 3: (A) CD data from *KIW7* solutions (0.5 mg/ml) containing only the peptide or preparations co-solubilized with SDS micelles. (B) CD spectra from *KIW7* samples (0.1 mg/ml) titrated with 200bp DNA at the indicated peptide-to-phosphate charge molar ratios. 200bp DNA spectrum (dashed line) is not to scale and is presented just a guide to the eye to allow comparison with peptide samples.

An interesting feature of *Penetratin* is appearance of random-to-β-sheet transitions upon interaction with anionic species, especially mimetic membrane models.[24,48] To investigate if these features are also found in the *KIW7* fragment, we measured CD spectra in samples containing SDS micelles. The spectrum shown in Figure 3A (open symbols) indicates a broad negative rotation centered at ~220 nm appearing upon interaction with micelles along with a shallow positive peak near to 203 nm, suggesting organization into β-sheets when *KIW7* associates with anionic surfactant interfaces.[18,49] Similar random-to-β-sheet transitions have been recently identified in *Penetratin* interacting with nucleic acids.[45] In Figure 3B, we show

CD spectra from a peptide solution titrated with concentrated 200bp DNA aliquots. The amount of DNA in the formulations has been chosen to range from a cationic peptide excess (2.7:1 molar ratio) up to an excess of anionic phosphate charges (1:2.2). Upon titration, spectra become quickly dominated by a strong positive peak at ~190 nm, which is very characteristic of *B*-form DNA.[46] *B*-form signature is also attested by a maximum at 210 nm and a minimum at 220 nm in CD spectrum from 200bp DNA solutions (dashed line in 3B). In addition to the strong rotation at 190 nm, data are characterized by increasing negative bands near to 223 nm, which indicates the emergence of β-sheet conformations upon interaction with anionic species. The presence of an isochoric point at 217 nm suggests two state cooperative transitions.[46,50]

The findings above demonstrate that *KIW7* shows that strong secondary structure similarity with *Penetratin*, suggesting that this heptameric fragment is crucial for the conformation of its parent sequence, and potentially plays a key role for non-covalent interactions with cell membranes and DNA cargoes.

X-ray, cryo-EM and AFM experiments: nanoscale structure

To extract detailed information on the nanoscopic structure of assemblies based on *KIW7* peptides, we have used complementary biophysical techniques comprising *in-situ* small-angle scattering (SAXS) in liquid medium and cryogenic transmission electron microscopy (cryo-TEM) on vitrified specimens, and *ex-situ* atomic force microscopy (AFM) and fiber X-ray diffraction on samples dried from peptide/pDNA solutions.

In SAXS experiments, the *q*-range investigated corresponds to lengths between 2 to 50 nm; therefore, the data provide insights into the supramolecular arrangement of the assemblies whereas microscopy give information on the morphology of the peptiplexes. In Figure 4A, we

show scattering curves from two samples, one of them containing only *KIW7* at 10 mg/ml and other with a mixture of peptides and 200bp DNA at equal molar charge ratio. Comparison between the curves straightforwardly shows that different aggregate structures are present in the solutions depending on the presence of DNA. Data from *KIW7* samples are characterized by a linear descent (in log-log representation) at low-q which is followed by a plateau at intermediate range and a new descent at higher q-values, denoting multiple structures across length scales corresponding to the SAXS data. These curves have been successfully fitted using a combination of a simple power law plus a Gaussian coil (GC) form factor. The power law exponent is associated to the slope found at low-q and it accounts for dimensionality of fractal aggregates in solution.[31,51] The GC form factor describes smaller structures in solution and it provides the gyration radius of scattering particles and the Flory parameter, which is correlated with interaction between these scatterers and solvent. The low-q scaling exponent has is α = -2.75, corresponding to mass fractals in solution,[31,52] and the radius of gyration and Flory parameter are R_g = 0.7 nm and ν = 0.35 respectively, consistent with free peptide chains collapsed in the solvent. These findings correlate well with CD assays which demonstrate that *KIW7* secondary structure is dominated by random coil conformations. In the case of *KIW7*/200bp DNA samples, the curves have been fitted using a long cylinder shell form factor.[35] The fitting parameters are R_c = 5.0 ± 2.8 nm and ΔS = 1.1 nm, respectively, for the core radius and shell thickness, which suggests a biomolecular core surrounded by a counterion shell. It should be noted that sizes found in SAXS assays indicate the presence of rod-like assemblies with total average diameter at 12.2 nm, thus much thicker than DNA duplexes.

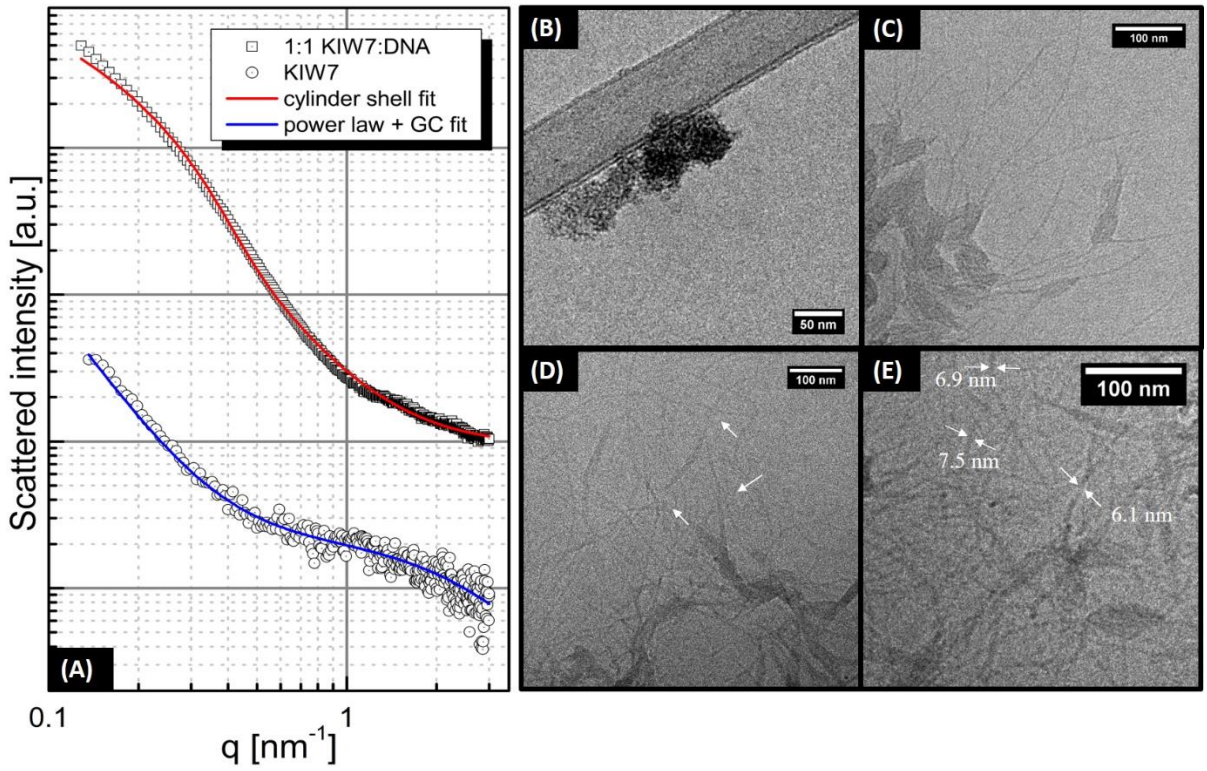

Figure 4: (A) SAXS profiles from preparations containing KIW7 at 10 mg/ml and different mixtures of KIW7/200bp DNA at 1:1 peptide-to-phosphate charge ratio. (B) micrograph from vitrified solution containing KIW7 at 10 mg/ml. (C) cryo-TEM image from KIW7/200bp DNA solution at 1:1 peptide-to-phosphate charge ratio. (D) and (E) images from KIW7/200bp DNA solutions at 2:1 charge ratio.

To further investigate the validity of SAXS fitting parameters, we have performed cryogenic transmission electron microscopy (cryo-TEM). Cryo-TEM is an *in-situ* technique that provides direct-space visualization of vitrified solutions containing peptiplexes at conditions very closeto those used in SAXS assays. Figure 4B shows a micrograph from *KIW7* solution at 10 mg/ml revealing only particles with irregular shapes in the samples, in agreement with SAXS data above that suggested the presence of fractal aggregates and unaggregated peptide chains. In Figure 4C, images from *KIW7*/DNA at 1:1 peptide-to-phosphate charge ratio display a richer polymorphism with consistent appearance of long unbranched fibers forming an interconnected network. Also, planar tape-like morphologies appear in co-existence with fibers. Images from samples containing *KIW7* and DNA at 2:1 charge ratio in Figure 4D also

reveal coexistence between fibrils and elongated tapes. Since fibrillar structures often appear as a continuation along the axis of nanotapes (white arrows), the tape-like assemblies could be due to lateral association between fibrils. At higher magnifications, Figure 4E, one observes that fibrillar assemblies possess thickness around 7 nm, compatible with sizes of polydisperse rod-like structures revealed by SAXS. Interestingly, lengths of the fibers easily reach a few hundred nanometers, whereas electrophoretic measurements indicate that DNA pieces are much shorter with ~ 200 bp (~ 67 nm). In this case, 200bp DNA duplexes likely behave as a scaffold directing fibrillization of *KIW7* peptide.

The finer structure of peptide/DNA fibers has been investigated through *ex-situ* approaches, namely, AFM and fiber X-rays measurements. To prepare the samples, we used calf thymus DNA with ~200 bp and plasmid DNA with 4.7 kb (pDNA). The AFM images in Figure clearly reveal the formation of an intricate network of fibers, similar to those revealed by *in-situ* techniques above. The sizes of the fibers are about 20 nm, a bit thicker than those observed in SAXS, probably due to differences in sample preparation between techniques. In Figure 5B, we observe that pDNA, which is a commonly used vector in gene therapy, also induces structuration of peptides into thin fibers. Overall, the morphology and dimensions of fibers formed by *KIW7*/pDNA are quite close to those found in samples prepared with 200bp DNA, indicating that a similar structuration pattern is present when long nucleotide sequences are used in the peptiplexes.

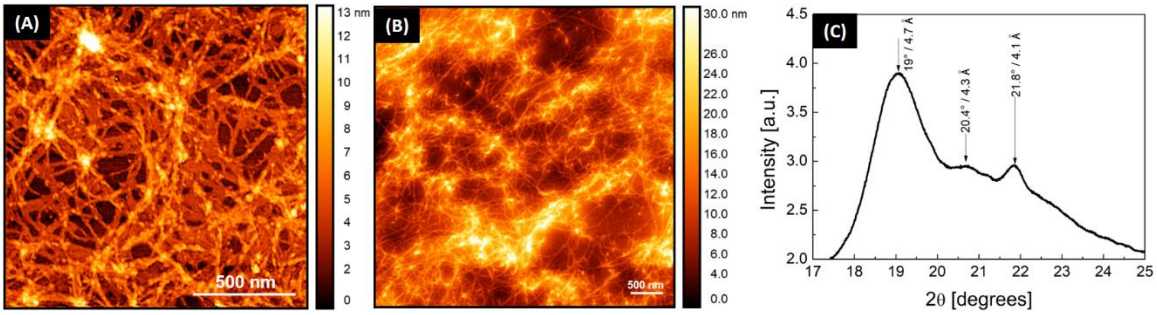

Figure 5: (A) AFM topography from *KIW7* peptide complexed (A) with 200bp DNA and (B) with pDNA. The formation of interconnected fiber networks is observed in both samples and the sizes of the structures are found to be around 20 nm, consistent with both cryo-EM and SAXS data. (C) Fiber X-ray diffraction performed on dried stalk from a solution containing *KIW7*/pDNA complexes. Packing into β-sheets is evidenced by the strong Bragg peak at $2\theta = 19°$ [CuK$_\alpha$].

To probe the molecular packing of these fibers, dried stalks were prepared from KIW7/pDNA solutions (1:1 molar ratio) and investigated by X-ray diffraction. The data, shown in Figure 5C, reveal three Bragg peaks at 2θ = 19°, 20.4 and 21.8°. The peak at 19° corresponds to a repeat distance of d = 4.7 Å, which is ascribed to the separation between hydrogen-bonded peptide strands organized into β-sheets.[53] The reflection at 2θ = 20.8° is associated with d = 4.3 Å and it reinforces the presence of β-sheets, since it agrees with the spacing between α-carbons in antiparallel β-sheets.[54] The third peak, 2θ = 21.8 °, arises from repeats with d = 4.1 Å which is frequent in peptide systems [32,55] and usually ascribed to separation between amino acid lateral chains.[56] As a whole, X-ray diffraction indicates that fibers exhibit β-sheet structure.

Structural model and self-assembly pathway for *KIW7*/DNA peptiplexes

From the data presented above, we are now in a position to elaborate a tentative model for describing the structure of *KIW7*/DNA peptiplexes. The proposed model is represented in Figure 6A showing a core-shell assembly where DNA double strands serve as a template for condensation of a peptide layer. This templating behavior of DNA agrees with previous observations in virus-like nanostructures,[57] and it resembles the spatial arrangement of inverted cylindrical micelles found in DNA/lipid complexes.[58] Since *KIW7* has cationic residues at both termini, condensation is likely triggered by electrostatic attraction between terminal amino acids and phosphates. In this case, we propose that peptide chains orient perpendicular to the long of the double helix forming an outer surface decorated with basic amino acids at the opposite side of peptide strands that makes fibers soluble. According to this arrangement, thickness of the fibers can be estimated by the sum of two extended heptameric chains (7 × 0.34 ~ 2.4 nm) plus the diameter of DNA duplexes (~2 nm),[36] resulting in a size of 6.8 nm, in close agreement with cryo-EM imaging and SAXS data. The model is fully consistent with β-sheets pairing as shown in Figure 6B, where hydrophobic effect and H-bonding between adjacent strands hold the assembly together. In addition, this spatial ordering enables π–π interactions between aromatic residues at neighbor peptides. In this case, phenylalanine and tryptophan π–stacks run parallel to the axis of the fiber and convey directionality for self-assembly,[59-61] thus complementing the template action exerted by DNA (see Figure 6C).

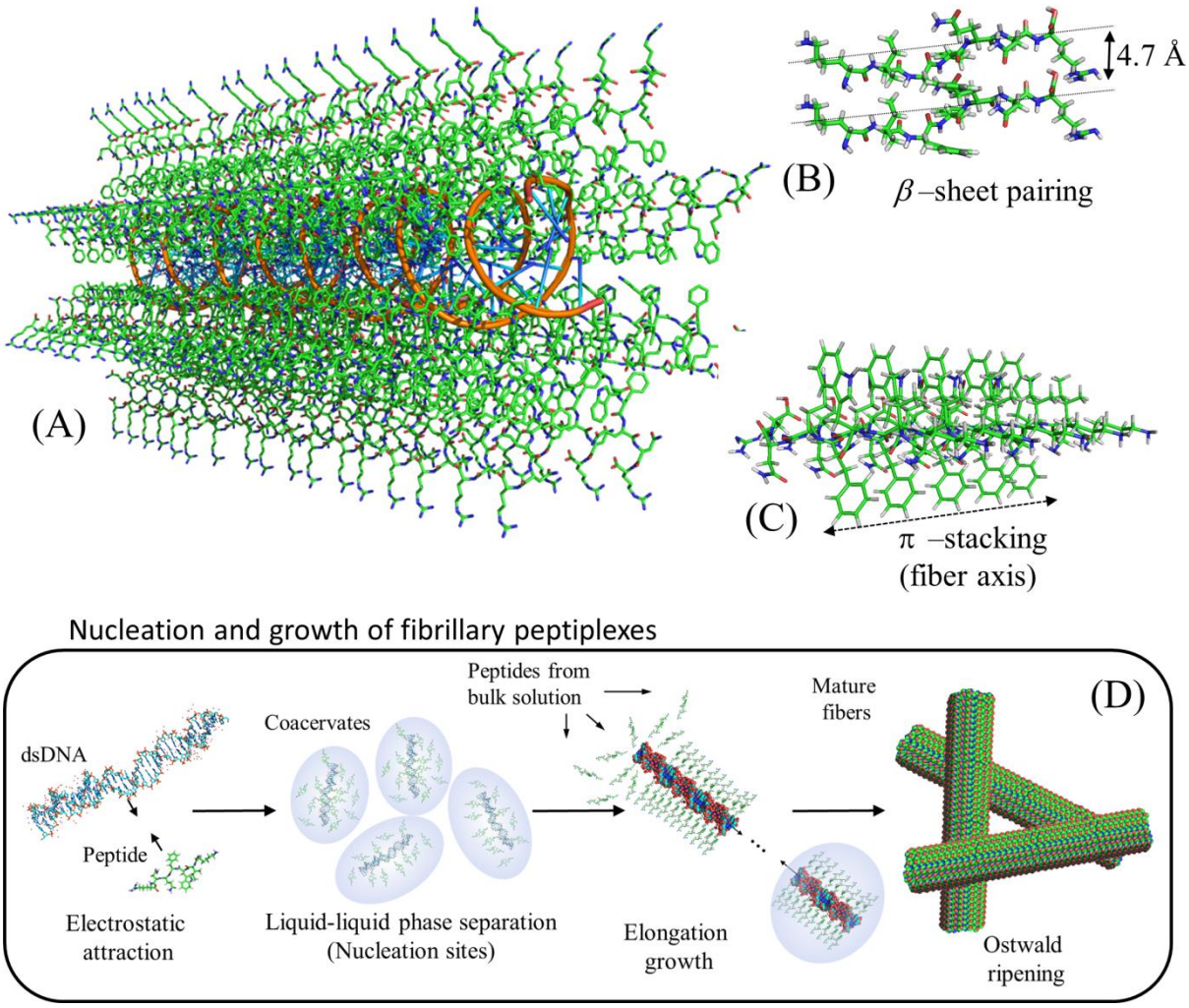

Figure 6: schematic representation of the structural model proposed for complexation between *KIW7* and DNA. (A) Fibrillary scaffold with a DNA core (orange ribbons) templating the growth of a peptide shell. (B) β–sheet paring between adjacent *KIW7* chains in the fibers. (C) Supramolecular stacks formed by π–π interactions between aromatic residues. (D) Illustration of nucleation and growth of peptiplexes through liquid-liquid phase separation.

The formation of fibrillary peptiplexes can be also viewed in the context of a nucleation-dependent polymerization mechanism.[62,63] Recently, nucleation and growth of peptide supramolecular polymers has been described to proceed through liquid-liquid phase separation,[62] and such a pathway can be used for explaining complexation between *KIW7* and DNA. This process is characterized by the formation of nucleation sites constituted by solute-

rich droplets from which the structures growth to further convert to thermodynamically stable nanofibers.[62,63] Our proposition for this pathway is schematically illustrated in Figure 6D, where it appears to be triggered by electrostatic attraction between peptides and DNA. As the next step, association between oppositely charged biomolecules leads to complex coacervation, with liquid-liquid phase separation generating droplets concentrated in DNA and peptides. In the following, these coacervates act as a nucleation center from which elongation of fibers is sustained by coalescence of clusters and incorporation of free biomolecules from bulk solution. Finally, the formation of mature fibers proceeds through usual Ostwald ripening with transient intermediates being added to thermodynamically stable long fibers.[62,63]

Cell assays: *KIW7* promotes cytosolic internalization of DNA fragments

Since *KIW7* is a fragment derived from *Penetratin*, a further step in our study has been to probe the interaction of this peptide with cell membranes and tentatively demonstrate its capacity to assist DNA delivery into HeLa cells. MTT assays have been performed for assessing cell viability in the presence of different concentrations of *KIW7*. These tests have been carried out using cells incubated during 4 hours with the peptide, the same incubation time used in delivery assays below, in agreement with protocols found elsewhere for *Penetratin.*[64] Also, 4 hours is a period longer than *Penetratin* plasma half-life observed *in vivo*.[65] Our results show that within this time lapse *KIW7* is well tolerated up to concentrations of 4 mg/ml, indicating low cytotoxicity (ESI file, Figure S3). In the following, we have prepared peptiplexes using *KIW7* peptide and 200bp DNA labelled with YOYO-1, a cell-impermeable dye that becomes highly fluorescent upon intercalation to DNA strands.[33,66] Therefore, by monitoring YOYO-1 fluorescence, we have been able to track the presence of exogenous DNA in cell culture. We incubated HeLa cells with *KIW7*/200bp DNA peptiplexes at a DNA

concentration of 5 μg per well at 1:1 or 2:1 molar ratio between peptide and phosphate charges, respectively. After 4 hours incubation, plates were rinsed to wash out unbonded 200bp DNA, and cells were fixed with paraformaldehyde for confocal microscopy assays. Two fluorescence channels have been investigated, one corresponding to DAPI blue-fluorescent dye staining nuclei, and the other associated to YOYO-1 green emission.

As shown in Figure 7, intense green fluorescence is observed throughout cells incubated with *KIW7*/200bp DNA complexes prepared at 2:1 molar ratio, indicating cell surface association of 200 bp DNA duplexes and showing that binding to cell membrane is facilitated when peptides are used in the formulation. When only labelled 200bp DNA is present in culture, the greener glow from YOYO-1 emission is not detected, indicating a complete (or almost complete) removal of non-specific binding.

In addition to association to cell surface, some degree of internalization is evidenced by the presence of exogenous DNA in the surroundings of nuclear membranes, as indicated by proximity between DAPI and YOYO-1 fluorescence, which denotes that 200bp DNA is anchored at eukaryotic barriers (bottom rows in Figure 7). To further investigate the distribution of DNA in the cells, we recorded images from different focal planes along the z-direction. The image series, shown in ESI file (video 1), reveals that fluorescence from 200bp DNA is found at different confocal planes, indicating that at least part of the nucleic acid payload enters cells when peptiplexes are formulated with *KIW7*. Although the data presented above do not allow for discriminating the pathways involved in the uptake, they indicate that binding of DNA to cell membranes, followed by penetration into cytosol, is assisted by peptiplexes based on *KIW7*. Interaction with cells has also been noticed for peptiplexes prepared at 1:1 charge ratio, however, at much lower intensities in comparison to samples where peptide excess was present (see ESI file, Fig. S5) which suggests that excess of cationic charges is relevant for cell binding and penetration.

Putting the findings above together, we observe that *KIW7* might be a suitable vector for preparing noncovalent complexes with DNA, where it could assist gene expression and regulate metabolism. Our data demonstrate that this short fragment containing the largest non-cationic portion of *Penetratin* promotes interaction with cell membranes for internalization, and potentially represents a cheaper and simpler CPP for cytosolic delivery of nucleic acids.

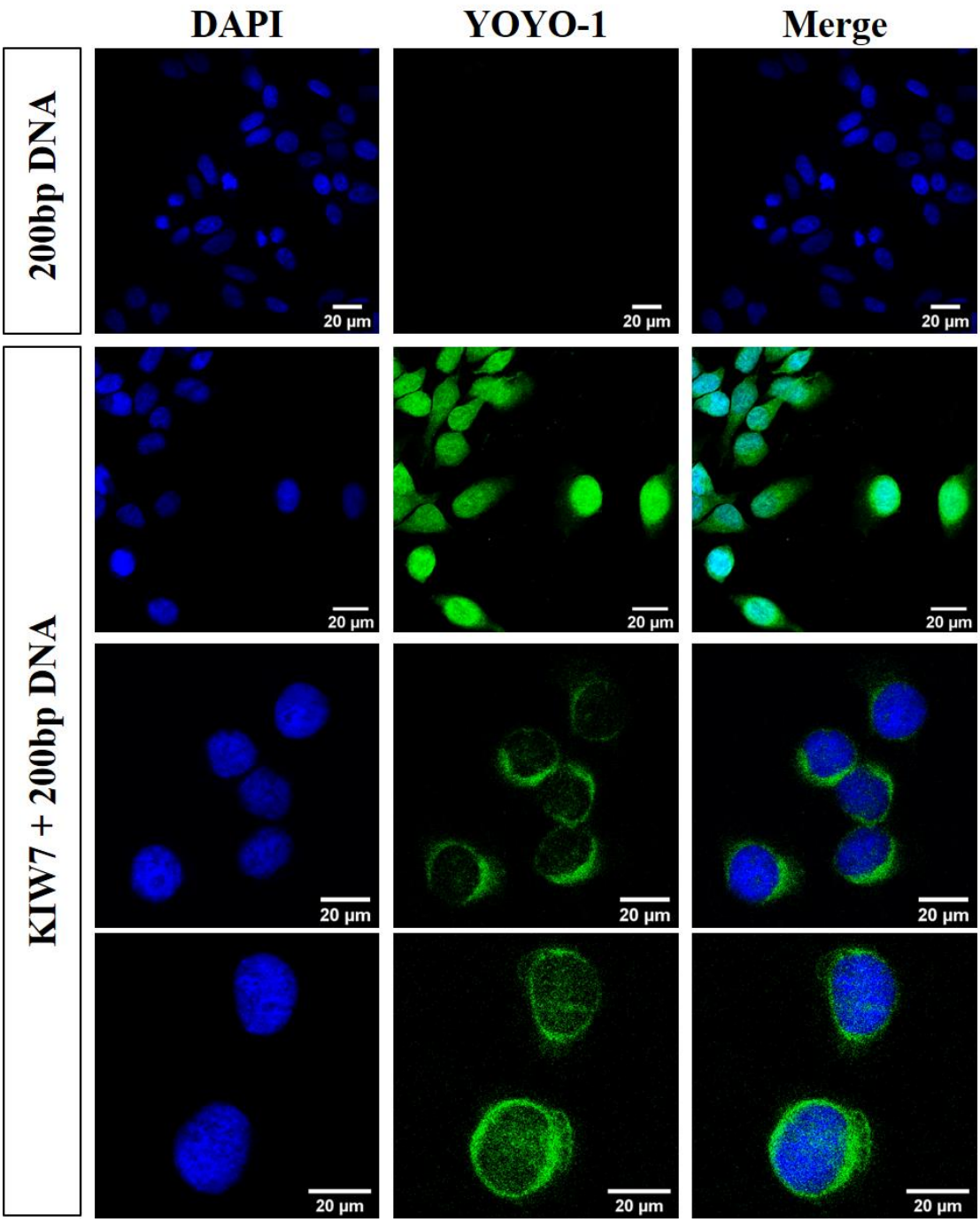

Figure 7: Confocal fluorescence images from HeLa cells incubated with *KIW7*/200bp DNA complexes at 2:1 peptide-to-phosphate charge ratio. DNA strands are stained with green YOYO-1 dye, whereas blue-fluorescent DAPI stains nuclei.

CONCLUSIONS

We have performed detailed investigations on both structure and cell membrane interaction of a heptamer derived from *Penetratin*, an archetypical *Trojan* peptide of great interest for biomedical research. The peptide has been successfully used to form peptiplexes with DNA, self-assembling into long nanofibers and nanotapes endowed with clear β-sheet features. The supramolecular structure of nanofibers likely comprises DNA cores surrounded by a peptide shell for which the double helix behaves as a template and induces fibrillization. A nucleation and growth mechanism proceeding through liquid-liquid phase separation of coacervates is proposed for describing the self-assembly of peptiplexes. We have demonstrated that *KIW7* is able to promote cell surface association and partially deliver DNA with ~200 bp into HeLa cells, indicating the potential of this truncated version of *Penetratin* for the transport of nucleotide sequences larger than those successfully transported by CPPs in recent reports.[67,68] In fact, 200bp DNA duplexes internalized with assistance of *KIW7* are about 10 times larger than microRNA and siRNA used to regulate cell metabolism and therefore *KIW7* is potentially suitable for delivery of these species or even oligonucleotides.

Since *KIW7* contains the longest non-cationic segment found in the *Penetratin* strand, it also represents an interesting model to probe the contribution of uncharged amino acids for overall structure of *Penetratin*. The capacity of the peptide to interact with anionic micelles was demonstrated even upon charge screening promoted by complexation with DNA, evidencing that hydrophobicity provided by IWF tripeptides in the middle of the strands are a key factor for interaction with biological membranes. In addition, *KIW7* conserves main features of *Penetratin* secondary structure, including random-to-β transitions upon interaction with anionic surfactant interfaces, thus suggesting that structuration of *Penetratin* in the presence of biomembranes (a key feature for translocation capacity) is closely correlated to the uncharged residues preserved in the truncated peptide. Although the role of non-polar amino acids for

bioactivity of *Trojan* peptides, specially tryptophan residues, has received increasingly attention in recent years,[20,35,69] the importance of cationic residues has been the main focus. In this context, the findings presented here undoubtably demonstrate that non-cationic amino acids are directly implicated in cell uptake and, even in the absence of strong cationicity, they make intracell delivery of DNA fragments feasible.

ACKNOWLEDGMENTS

This project has been supported by FAPESP under process nº 2016/24409-3 granted to ERS, who is also a fellow of the National Council for Scientific and Technological Development – CNPq (Proc. N° 310916/2019-4). LRM has been supported by a doctoral fellowship from CAPES-Proex granted to the Graduate Program in Molecular Biology of UNIFESP (Finance Code 001). SAXS data has been collected at the Brazilian National Synchrotron Laboratory-LNLS under proposal 20170958. IWH and VC acknowledge EPSRC for Platform grant EP/L020599/1. This work has been partially supported by the UNIFESP CAPES-PrInt program in the theme "Development of treatment and therapeutics for inflammatory diseases". WAA is supported by CNPq (grant n° 304389/2019-6), the National Institute of Science and Technology in Bioanalytics (FAPESP grant no. 2014/50867-3 and CNPq grant no. 465389/2014-7), and FAPESP (grant nos. 2015/24018-1, 2017/02317-2). AFM and cryo-TEM experiments have been conducted at the National Nanotechnology Laboratory – LNNano under proposals AFM-36338 and TEM-24500. We are very grateful to Drs. Florian Meneau (SAXS1-LNLS), Carlos Costa (AFM-LNNano) and Antonio Borges (TEM-LNNano) for kind assistance during data collection.

REFERENCES

1 S. Guha, J. Ghimire, E. Wu and W. C. Wimley, *Chem. Rev.*, 2019, **119**, 6040–6085.

2 I. W. Hamley, *Chem. Rev.*, 2017, **117**, 14015–14041.

3 K. Kurrikoff and U. Langel, *Expert Opin. Drug Deliv.*, 2019, **16**, 1183–1191.

4 A. D. Frankel and C. O. Pabo, *Cell*, 1988, **55**, 1189–1193.

5 A. Joliot, C. Pernelle, H. Deagostini-Bazin and A. Prochiantz, *Proc. Natl. Acad. Sci.*, 1991, **88**, 1864–1868.

6 D. Derossi, A. H. Joliot, G. Chassaing and A. Prochiantz, *J. Biol. Chem.*, 1994, **269**, 10444–10450.

7 J. S. Bahnsen, H. Franzyk, E. J. Sayers, A. T. Jones and H. M. Nielsen, *Pharm. Res.*, 2015, **32**, 1546–1556.

8 B. Raudszus, D. Mulac and K. Langer, *Int. J. Pharm.*, 2018, **536**, 211–221.

9 C. Liu, K. Jiang, L. Tai, Y. Liu, G. Wei, W. Lu and W. Pan, *ACS Appl. Mater. Interfaces*, 2016, **8**, 19256–19267.

10 X. Xie, J. E. Kerrigan, T. Minko, O. Garbuzenko, K. C. Lee, A. Scarborough, E. E. Abali, T. Budak-Alpdogan, N. Johnson-Farley, D. Banerjee, K. W. Scotto and J. R. Bertino, *Cancer Biol. Ther.*, 2013, **14**, 742–751.

11 T. Yin, W. Xie, J. Sun, L. Yang and J. Liu, *ACS Appl. Mater. Interfaces*, 2016, **8**, 19291–19302.

12 N. Skrlj, G. Drevensek, S. Hudoklin, R. Romih, V. Curin Serbec and M. Dolinar, *Appl Biochem Biotechnol*, 2013, **169**, 159–169.

13 K. Jiang, X. Gao, Q. Shen, C. Zhan, Y. Zhang, C. Xie, G. Wei and W. Lu, *Acta Biomater.*, 2017, **63**, 123–134.

14 L. Tai, C. Liu, K. Jiang, X. Chen, G. Wei, W. Lu and W. Pan, *Nanomedicine-Nanotechnology Biol. Med.*, 2017, **13**, 2091–2100.

15 X. Q. Xie, N. Bansal, T. Shaik, J. E. Kerrigan, T. Minko, O. Garbuzenko, E. E. Abali, N.

Johnson-Farley, D. Banerjee, K. W. Scotto and J. R. Bertino, *Oncotarget*, 2014, **5**, 901–907.

16 I. Nakase, H. Akita, K. Kogure, A. Graslund, U. Langel, H. Harashima and S. Futaki, *Acc. Chem. Res.*, 2012, **45**, 1132–1139.

17 C. J. Chene and W. M. Saltzman, *Biomaterials*, 2011, **32**, 6194–6203.

18 D. Kalafatovic and E. Giralt, *Molecules*, 2017, **22**, 1929.

19 E. Dupont, A. Prochiantz and A. Joliot, in *Cell-Penetrating Peptides: Methods and Protocols*, ed. Ü. Langel, Humana Press, Totowa, NJ, 2011, pp. 21–29.

20 P. Gehan, V. Vivier, K. Ngo, S. Sagan, A. Walrant, S. Cribier and N. Rodriguez, *Biophys. J.*, 2020, **118**, 383a.

21 I. D. Alves, N. Goasdoué, I. Correia, S. Aubry, C. Galanth, S. Sagan, S. Lavielle and G. Chassaing, *Biochim. Biophys. Acta - Gen. Subj.*, 2008, **1780**, 948–959.

22 C.-Y. Jiao, E. Sachon, I. D. Alves, G. Chassaing, G. Bolbach and S. Sagan, *Angew. Chemie Int. Ed.*, 2017, **56**, 8226–8230.

23 H. Binder and G. Lindblom, *Biophys J*, 2003, **85**, 982–995.

24 H. Binder and G. Lindblom, *Biophys J*, 2004, **87**, 332–343.

25 G. Drin, H. Déméné, J. Temsamani and R. Brasseur, *Biochemistry*, 2001, **40**, 1824–1834.

26 W. B. Kauffman, T. Fuselier, J. He and W. C. Wimley, *Trends Biochem. Sci.*, 2015, **40**, 749–764.

27 E. Eiríksdóttir, K. Konate, Ü. Langel, G. Divita and S. Deshayes, *Biochim. Biophys. Acta - Biomembr.*, 2010, **1798**, 1119–1128.

28 C. Bechara and S. Sagan, *Febs Lett.*, 2013, **587**, 1693–1702.

29 H. A. Rydberg, M. Matson, H. L. Åmand, E. K. Esbjörner and B. Nordén, *Biochemistry*, 2012, **51**, 5531–5539.

30 M.-L. Jobin, M. Blanchet, S. Henry, S. Chaignepain, C. Manigand, S. Castano, S.

Lecomte, F. Burlina, S. Sagan and I. D. Alves, *Biochim. Biophys. Acta - Biomembr.*, 2015, **1848**, 593–602.

31 E. R. Silva, E. Listik, S. W. Han, W. A. Alves, B. M. Soares, M. Reza, J. Ruokolainen and I. W. Hamley, *Biophys. Chem.*, 2018, **233**, 1–12.

32 C. C. Decandio, E. R. Silva, I. W. Hamley, V. Castelletto, M. S. Liberato, V. X. Oliveira, C. L. P. Oliveira and W. A. Alves, *Langmuir*, 2015, **31**, 4513–4523.

33 E. R. T. da Silva, E. A. de Oliveira, A. Fevrier, F. Nallet and L. Navailles, *Eur Phys J E Soft Matter*, 2011, **34**, 83.

34 E. A. de Oliveira, E. R. T. da Silva, A. Fevrier, E. Grelet, F. Nallet, L. Navailles, E. A. de Oliveira, E. R. T. da Silva, A. Février, G. É, F. Nallet and L. Navailles, *Epl*, 2010, **91**, 28001.

35 E. R. Silva, G. Cooney, I. W. Hamley, W. A. Alves, S. Lee, B. F. O'Connor, M. Reza, J. Ruokolainen and D. Walls, *Soft Matter*, 2016, **12**, 9158–9169.

36 H. H. Strey, R. Podgornik, D. C. Rau and V. A. Parsegian, *Curr. Opin. Struct. Biol.*, 1998, **8**, 309–313.

37 D. W. Sambrook, Joseph; Russell, *Molecular cloning : a laboratory manual*, Cold Spring Harbor Laboratory Press, Cold Spring Harbor, N.Y, 3rd edn., 2001.

38 B. M. Soares, A. M. Aguilar, E. R. Silva, M. D. Coutinho-Neto, I. W. Hamley, M. Reza, J. Ruokolainen and W. A. Alves, *Phys. Chem. Chem. Phys.*, 2017, **19**, 1181–1189.

39 J. R. Lakowicz, *Principles of Fluorescence Spectroscopy* , Springer, New York, 4th edn., 2006.

40 D. V Tulumello and C. M. Deber, *Biochemistry*, 2009, **48**, 12096–12103.

41 M. H. Shabestari, N. J. Meeuwenoord, D. V Filippov and M. Huber, *J. Biol. Phys.*, 2016, **42**, 299–315.

42 J.-M. Lin, T.-L. Lin, U.-S. Jeng, Z.-H. Huang and Y.-S. Huang, *Soft Matter*, 2009, **5**, 3913–3919.

43 A. Wahlström, L. Hugonin, A. Perálvarez-Marín, J. Jarvet and A. Gräslund, *FEBS J.*,

2008, **275**, 5117–5128.

44 K. Kilk, M. Magzoub, M. Pooga, L. E. G. Eriksson, Ü. Langel and A. Gräslund, *Bioconjug. Chem.*, 2001, **12**, 911–916.

45 L. R. De Mello, I. W. Hamley, V. Castelletto, B. B. M. Garcia, S. W. Han, C. L. P. De Oliveira and E. R. Da Silva, *J. Phys. Chem. B*, 2019, **123**, 8861–8871.

46 B. Nordén, A. Rodger, T. Dafforn and Royal Society of Chemistry (Great Britain), *Linear dichroism and circular dichroism : a textbook on polarized-light spectroscopy*, Royal Society of Chemistry, Cambridge, 2010.

47 M. J. Krysmann, V. Castelletto, A. Kelarakis, I. W. Hamley, R. A. Hule and D. J. Pochan, *Biochemistry*, 2008, **47**, 4597–4605.

48 J. Ye, S. A. Fox, M. Cudic, E. M. Rezler, J. L. Lauer, G. B. Fields and A. C. Terentis, *J. Am. Chem. Soc.*, 2010, **132**, 980–988.

49 H. L. Åmand, H. A. Rydberg, L. H. Fornander, P. Lincoln, B. Nordén and E. K. Esbjörner, *Biochim. Biophys. Acta - Biomembr.*, 2012, **1818**, 2669–2678.

50 E. R. da Silva, W. A. Alves, V. Castelletto, M. Reza, J. Ruokolainen, R. Hussain and I. W. Hamley, *Chem. Commun.*, 2015, **51**, 11634–11637.

51 T. Zemb and P. Lindner, *Neutrons, X-rays and light : scattering methods applied to soft condensed matter*, Elsevier, Amsterdam ; Boston, 1st edn., 2002.

52 G. Beaucage, *J. Appl. Crystallogr.*, 1996, **29**, 134–146.

53 K. E. Marshall and L. C. Serpell, *Biochem. Soc. Trans.*, 2009, **37**, 671–676.

54 A. Baumketner, S. L. Bernstein, T. Wyttenbach, N. D. Lazo, D. B. Teplow, M. T. Bowers and J.-E. Shea, *Protein Sci.*, 2006, **15**, 1239–1247.

55 O. S. Makin and L. C. Serpell, *J. Mol. Biol.*, 2004, **335**, 1279–1288.

56 P. Sikorski, E. D. T. Atkins and L. C. Serpell, *Structure*, 2003, **11**, 915–926.

57 Y. Ruff, T. Moyer, C. J. Newcomb, B. Demeler and S. I. Stupp, *J. Am. Chem. Soc.*, 2013, **135**,6211-6219.

58 I. Koltover, T. Salditt, J. O. Radler and C.R. Safynia, *Science*, 1998, **281**, 78-81.

59 Y. Lin, Y. Qiao, P. Tang, Z. Li and J. Huang, *Soft Matter*, 2011, **7**, 2762-2769.

60 J. Li, R. Xing, S. Bai and X. Yan, *Soft Matter*, 2019, **15**, 1704-1715.

61 C. Yuan, W. Ji, R. Xing, J. Li, E. Gazit and X. Yan, *Nat. Rev. Chem.*, 2019, **3**, 567-588.

62 C. Yuan, A. Levin, W. Chen, R. Xing, Q. Zou, T. W. Herling, P. K. Challa, T. P. J. Knowles and X. Yan, *Angew. Chem. Int.*, 2019, **58**, 18116-18123.

63 J. Wang, K. Liu, R. Xing and X. Yan, *Chem. Soc. Rev.*, 2016, **45**, 5589-5604.

64 B. Christiaens, J. Grooten, M. Reusens, A. Joliot, M. Goethals, J. Vandekerckhove, A. Prochiantz and M. Rosseneu, *Eur. J. Biochem.*, 2004, **271**, 1187-1197.

65 E. J. B. Nielsen, S. Yoshida, N. Kamei, R. Iwamae, E.S. Khafaby, J. Olsen, U. L. Rahbek, B. L. Pedersen, K. Takayama and M. T. Morishita, *J. Control. Release*, 2014, **189**, 19-24.

66 B. Kundukad, J. Yan and P. S. Doyle, *Soft Matter*, 2014, **10**, 9721–9728.

67 W. B. Kauffman, S. Guha and W. C. Wimley, *Nat. Commun.*, 2018, **9**, 2568.

68 S. Tarvirdipour, C.-A. Schoenenberger, Y. Benenson and C. G. Palivan, *Soft Matter*, 2020, **16**, 1678–1691.

69 A. Walrant, A. Bauzá, C. Girardet, I. D. Alves, S. Lecomte, F. Illien, S. Cardon, N. Chaianantakul, M. Pallerla, F. Burlina, A. Frontera and S. Sagan, *Biochim. Biophys. Acta - Biomembr.*, 2020, **1862**, 183098.

ToC Entry